Phys Chem Minerals (1994) 21:156–165

PHYSICS AND CHEMISTRY OF MINERALS

Kinetics of Diffusion-Controlled Growth of Fayalite

D.K. Fisler and S.J. Mackwell

Department of Geosciences, Pennsylvania State University, University Park, PA 16802, USA

Received April 29, 1993 / Revised, accepted November 3, 1993

Abstract. The rate of growth of fayalite (Fe_2SiO_4) has been measured at one atmosphere total pressure, temperatures from 1000° to 1120° C, and oxygen fugacities controlled by CO/CO_2 gas-mixing from $10^{-9.9}$ to $10^{-13.0}$ atm, chosen to span the fayalite stability field. The fine-grained polycrystalline fayalite layer was formed by reacting the oxides FeO or Fe_3O_4 with a thin slice of single-crystal quartz. The rate of growth of the fayalite increases with increasing temperature and decreasing oxygen fugacity, and is consistent with a parabolic rate law, indicating that the growth rate is controlled by diffusion through the fayalite. Microstructural observations and platinum marker experiments suggest that the reaction phase is formed at the quartz-fayalite interface, and is therefore controlled by the diffusion of iron and oxygen. The parabolic rate constant was analyzed in terms of the oxide activity gradient to yield mean chemical diffusivities for the rate-limiting ionic species, assuming bulk transport through the fayalite layer. Given that iron diffusion in olivine polycrystals occurs either by lattice diffusion, which shows a positive dependence on oxygen activity, or by grain boundary diffusion, which would result in growth rates significantly faster than we observe, we conclude that the diffusivities derived in this study represent oxygen diffusion. However, since oxygen lattice diffusion in fayalite has been established to be much slower than our measurements, it is likely that the transport path for oxygen is along the grain boundaries. Thus, the mean grain boundary diffusivity of oxygen in fayalite $\bar{D}^{gb}_O$ ($m^2\,s^{-1}$), using the measured grain size of 0.25 μm, is then given by

$$\bar{D}^{gb}_O\,\delta = 1.28 \times 10^{-3} f_{O_2}^{-0.17} e^{-540/RT},$$

where δ is the grain boundary width (in m), and the activation energy is in kJ/mol. Assuming $\delta = 10^{-9}$ m (Ricoult and Kohlstedt 1983), the oxygen grain boundary diffusivities are about a factor of 30 × slower than those reported by Watson (1986) for Fo_{90} olivine.

Introduction

The rate at which mechanical and physical processes occur in the Earth's mantle is controlled by the transport of ionic and electronic species. Since diffusion rates along grain boundaries are typically several orders of magnitude faster than lattice diffusivities (e.g. Atkinson and Taylor 1981), transport-limited processes such as creep, conductivity, phase transformations, and recrystallization may be controlled by grain boundary diffusion.

Although measurements of ionic diffusion along grain boundaries have been made for a number of oxides (e.g. Atkinson 1987; Atkinson and Taylor 1979, 1981, 1982, 1985), there have been comparatively few measurements for geologic materials. Studies of grain boundary diffusion of oxygen in quartzite (Farver and Yund 1991), and in dunite (Watson 1986) confirm that grain boundaries in rocks can provide fast diffusion paths for some ionic species. By contrast, tracer diffusivities for iron in polycrystalline olivine with average grain sizes of 50 μm or larger are the same as those in single crystals (Hermeling and Schmalzried 1984), indicating that grain boundaries did not necessarily provide a fast transport path for iron.

Since olivine with an approximate composition $(Mg_{0.9}Fe_{0.1})_2SiO_4$ is generally accepted to be the major constituent of the upper mantle of the Earth, its mechanical and physical behavior is expected to dominate the properties of this region. It is evident from a comparison of creep and diffusion data for olivine with those for forsterite (Mg_2SiO_4) and fayalite (Fe_2SiO_4) that the behavior of natural olivine more closely approximates that of fayalite. Consequently, to understand defect-controlled transport properties in the mantle, it is important to study the transport properties of fayalite.

A number of previous studies have measured cation diffusion in olivine of different compositions ($(Mg_{1-x}Fe_x)_2SiO_4$, where $x = 0.0$ to 1.0, corresponding to Fo_{100} to Fo_0). Jurewicz and Watson (1988) determined diffusion rates for Fe, Mg, Mn, and Ca in natural Fo_{90} olivine. Diffusion rates for Fe–Mg interdiffusion were measured by Buening and Buseck (1973) and Mis-

ener (1972, 1974) in olivine single crystals, and by Nakamura and Schmalzried (1984) in synthetic polycrystalline olivine. The positive dependence of cation diffusion rates on oxygen fugacity reported by Buening and Buseck (1973) and Nakamura and Schmalzried (1984) indicates that diffusion of iron and magnesium is vacancy-controlled. In a complementary study by Hermeling and Schmalzried (1984) tracer diffusion rates for iron were measured for a range of compositions of synthetic polycrystalline olivine and a natural single crystal of San Carlos Fo_{90} ($(Mg_{0.9}Fe_{0.1})_2SiO_4$) olivine. The agreement between the diffusivities for single crystals and polycrystals in these studies implies that iron lattice diffusion in olivine is at least as fast as grain boundary diffusion at coarse (~ 50 μm and 100–150 μm) grain sizes. Watson (1991) also reports iron diffusivities in natural olivine polycrystals. However, he observed transport rates for iron along grain boundaries that were faster than in the lattice for finer (< 66 μm and ~ 12 μm) grain sizes.

Reddy et al. (1080) and Jaoul et al. (1980, 1983) performed diffusion experiments with oxygen tracers in single-crystal Fo_{100} forsterite. These experiments show that the diffusion of oxygen in forsterite is much slower than that of iron or magnesium in olivine. More significantly, oxygen diffusion in these studies showed no dependence on f_{O_2}. In contrast, the diffusion of oxygen in natural Fo_{90} olivine, measured by Ryerson et al. (1989) and Gerard and Jaoul (1989) is two to three orders of magnitude faster than in forsterite and shows a positive dependence on oxygen activity, indicating an interstitial diffusion mechanism.

Watson (1986) performed high-pressure experiments on oxygen grain boundary diffusion in a synthetic dunite. The experimental configuration involved crushed San Carlos olivine in an oxygen potential gradient resulting from the difference between the oxygen activity of the reducing container (iron) and an oxidizing phase (hematite) dispersed throughout the crushed olivine or located as a central pellet. Diffusion rates were derived from the rate of increase, following sintering, of the magnetite zone (reduced from hematite) that was formed by the diffusion of oxygen down the potential gradient from the hematite to the iron container. These experiments revealed diffusivities that were significantly higher than those derived from single crystal experiments.

Silicon diffusion in single crystals of forsterite and olivine has been measured by Jaoul et al. (1981) and Houlier et al. (1988, 1990), respectively, and is slower than oxygen and iron diffusion under their experimental conditions. In forsterite, silicon diffusivities are independent of oxygen fugacity. By contrast, in Fo_{90} olivine the oxygen fugacity exponent is negative, indicating that silicon diffusion occurs by an interstitial mechanism. No diffusion rates have previously been measured for oxygen or silicon along grain boundaries in olivine samples that were initially fully dense.

Growth Kinetics

The reaction between quartz and iron oxide to form fayalite can be treated as a reaction between two binary phases to form a single ternary phase by a solid-solid reaction such as $2AO + BO_2 \rightleftarrows A_2BO_4$ (Schmalzried 1978). Once a continuous fayalite rim has formed from the reaction between the two minerals, diffusion through the rim is required for further growth. If the kinetics are controlled by the reaction at an interface, the thickness of the fayalite will increase linearly with increasing time. If diffusion is the rate-limiting process, the growth of the fayalite rim will obey a parabolic rate law. For the latter case, the relationship between the rim thickness and time can be calculated as follows using a formalism similar to that presented in Schmalzried (1978) and Borchardt et al. (1979).

From Fick's first law of diffusion, the flux j_i of chemical species i in an electrochemical potential gradient $\nabla\eta_i$ is given by

$$j_i = -\frac{D_i C_i}{RT} \nabla\eta_i, \tag{1}$$

where C_i is the concentration of species i and D_i is the partial chemical diffusivity of the species. The gradient in electrochemical potential can be written in terms of the gradient in chemical potential μ_i and electrical potential ϕ:

$$\nabla\eta_i = \nabla\mu_i + zF\nabla\phi, \tag{2}$$

where z is the charge on species i and F is the Faraday constant.

For the specific case of the formation of a layer of fayalite (Fe_2SiO_4) by the reaction between wüstite (FeO) and quartz (SiO_2),

$$2FeO + SiO_2 \rightleftarrows Fe_2SiO_4,$$

we can write flux equations for the transport of the ionic species through the fayalite, assuming one dimensional diffusion parallel to x,

$$j_{Fe^{2+}} = -\frac{D_{Fe} C_{Fe}}{RT} \frac{d}{dx} (\mu_{Fe^{2+}} + 2F\phi) \tag{3a}$$

$$j_{O^{2-}} = -\frac{D_O C_O}{RT} \frac{d}{dx} (\mu_{O^{2-}} - 2F\phi) \tag{3b}$$

$$j_{Si^{4+}} = -\frac{D_{Si} C_{Si}}{RT} \frac{d}{dx} (\mu_{Si^{4+}} + 4F\phi). \tag{3c}$$

If the rate of growth of the fayalite layer is diffusion- rather than interface-controlled, it will be dependent on the diffusivities of the two more mobile ionic species. Growth can occur by the coupled diffusion of iron and oxygen from the wüstite-fayalite interface to the quartz-fayalite interface, by the coupled diffusion of silicon and oxygen from the quartz-fayalite interface to the wüstite-fayalite interface, or by counterdiffusion of iron and silicon within the fayalite, transporting silicon to the wüstite-fayalite interface and iron to the quartz-fayalite interface. Thus, in the theoretical treatments given below, we will assume that the mobile species are either (a) iron and oxygen, (b) oxygen and silicon, or (c) iron and silicon,

with the third species in each case being treated as immobile.

(a) Coupled Diffusion of Iron and Oxygen

If we assume that silicon is essentially immobile within the fayalite, so that the growth of the fayalite occurs by diffusion of iron and oxygen ions from the wüstite-fayalite interface through the fayalite to the quartz-fayalite interface, the fluxes of iron and oxygen will be coupled to maintain stoichiometry:

$$j_{Fe^{2+}} = j_{O^{2-}}.$$

From (3a) and (3b), it can be shown that

$$D_{Fe} C_{Fe}(d\mu_{Fe^{2+}} + 2F\,d\phi) = D_O C_O(d\mu_{O^{2-}} - 2F\,d\phi)$$

and

$$-2F\,d\phi = \frac{D_{Fe} C_{Fe}\,d\mu_{Fe^{2+}} - D_O C_O\,d\mu_{O^{2-}}}{D_{Fe} C_{Fe} + D_O C_O}.$$

Thus,

$$j_{O^{2-}} = j_{Fe^{2+}} = -\frac{1}{RT}\frac{D_O C_O D_{Fe} C_{Fe}}{D_O C_O + D_{Fe} C_{Fe}}\frac{(d\mu_{Fe^{2+}} + d\mu_{O^{2-}})}{dx}$$

and, since $\mu_{Fe^{2+}} + \mu_{O^{2-}} = \mu_{FeO}$,

$$j_{O^{2-}} = j_{Fe^{2+}} = -\frac{1}{RT}\frac{D_O C_O D_{Fe} C_{Fe}}{D_O C_O + D_{Fe} C_{Fe}}\frac{d\mu_{FeO}}{dx}. \tag{4}$$

Now, in fayalite, $2C_{Fe} = C_O$. Also, the chemical potentials of wüstite and silica across the fayalite vary from $\mu_{FeO} = \mu^0_{FeO}$ ($a_{FeO} = 1$) and $\mu_{SiO_2} = \mu'_{SiO_2}$ (the chemical potential of silica in fayalite when $a_{FeO} = 1$) at $x = 0$ (the wüstite-fayalite interface), to $\mu_{FeO} = \mu'_{FeO}$ (the chemical potential of wüstite in fayalite when $a_{SiO_2} = 1$) and $\mu_{SiO_2} = \mu^0_{SiO_2}$ ($a_{SiO_2} = 1$) at $x = \Delta x$ (the quartz-fayalite interface). Integrating (4) across the fayalite layer yields

$$\int_{x=0}^{\Delta x} j_{O^{2-}}\,dx = -\frac{C_O}{RT}\int_{\mu^0_{FeO}}^{\mu'_{FeO}} \frac{D_O D_{Fe}}{2D_O + D_{Fe}}\,d\mu_{FeO}. \tag{5}$$

As there are no sources or sinks for oxygen across the fayalite, $j_{O^{2-}}$ is a constant. If we assume, on the basis of the rapid diffusivities reported for iron in olivine (Hermeling and Schmalzried 1984; Watson 1991), that iron diffuses much faster than oxygen, so that $D_O \ll D_{Fe}$,

$$\int_{\mu^0_{FeO}}^{\mu'_{FeO}} \frac{D_O D_{Fe}}{2D_O + D_{Fe}}\,d\mu_{FeO} \approx \int_{\mu^0_{FeO}}^{\mu'_{FeO}} D_O\,d\mu_{FeO}.$$

Using the Mean-Value Theorem, we can write the mean value of the oxygen diffusivity across the fayalite, $\bar{D}_O$, as

$$\bar{D}_O = \frac{1}{\Delta\mu_{FeO}}\int_{\mu^0_{FeO}}^{\mu'_{FeO}} D_O\,d\mu_{FeO}$$

where $\Delta\mu_{FeO} = \mu'_{FeO} - \mu^0_{FeO}$. At $x = \Delta x$ (the quartz-fayalite interface), where new fayalite molecules are formed, $\mu_{FeO} = \mu'_{FeO}$ and $\mu_{SiO_2} = \mu^0_{SiO_2}$. Thus, the Gibbs free energy of formation of fayalite from the oxides $\Delta G^0_{Fe_2SiO_4}$ is given by

$$\begin{aligned}\Delta G^0_{Fe_2SiO_2} &= 2(\mu_{FeO} - \mu^0_{FeO}) + (\mu_{SiO_2} - \mu^0_{SiO_2}) \\ &= 2(\mu'_{FeO} - \mu^0_{FeO}) = 2\Delta\mu_{FeO}\end{aligned}$$

and (5) can be rewritten as

$$j_{O^{2-}}\,\Delta x = -\frac{C_O \bar{D}_O}{2RT}\Delta G^0_{Fe_2SiO_4}. \tag{6}$$

Now, the flux j_i of the species that regulates growth is related to the thickness Δx of the fayalite layer as:

$$\frac{d\Delta x}{dt} = j_i V_m \xi \tag{7}$$

where V_m is the molar volume of the fayalite and ξ is a stoichiometric coefficient defined as the number of moles of fayalite formed due to the transport of one mole of species i. Thus, for the growth of a fayalite layer, where oxygen diffusion is rate-limiting, we can combine (6) and (7) to give

$$\frac{d\Delta x}{dt} = -\frac{C_O \bar{D}_O V_m \xi}{2\Delta x}\frac{\Delta G^0_{Fe_2SiO_4}}{RT}. \tag{8}$$

Given that, for fayalite $C_O = 4/V_m$, $\xi = \frac{1}{2}$ mole of fayalite formed per mole of oxygen diffused through the layer, and integrating (8) across the fayalite layer yields

$$\int_{x=0}^{\Delta x} \Delta x\,d\Delta x = -\bar{D}_O\frac{\Delta G^0_{Fe_2SiO_4}}{RT}\int_{t=0}^{t} dt.$$

Thus, for $D_{Si} \ll D_O \ll D_{Fe}$,

$$(\Delta x)^2 = -2\bar{D}_O\frac{\Delta G^0_{Fe_2SiO_4}}{RT}t. \tag{9}$$

If, by contrast, $D_{Si} \ll D_{Fe} \ll D_O$ we could perform a similar calculation using (5) to show that

$$(\Delta x)^2 = -\bar{D}_{Fe}\frac{\Delta G^0_{Fe_2SiO_4}}{RT}t. \tag{10}$$

(b) Coupled Diffusion of Silicon and Oxygen

If we assume that iron is essentially immobile within the fayalite, so that the growth of the fayalite occurs by diffusion of silicon and oxygen ions from the quartz-fayalite interface through the fayalite to the wüstite-fayalite interface, the fluxes of silicon and oxygen will be coupled to maintain stoichiometry:

$$2j_{Si^{4+}} = j_{O^{2-}}$$

and, since $\mu_{Si^{4+}} + 2\mu_{O^{2-}} = \mu_{SiO_2}$, (4) can be rewritten as

$$j_{O^{2-}} = 2j_{Si^{4+}} = -\frac{2}{RT}\frac{D_O C_O D_{Si} C_{Si}}{D_O C_O + 4D_{Si} C_{Si}}\frac{d\mu_{SiO_2}}{dx}.$$

Let us assume that $D_{Fe} \ll D_O \ll D_{Si}$. Following similar arguments to those presented above, we can show that, as $4C_{Si} = C_O = 4/V_m$ and $\xi = \frac{1}{2}$ mole of fayalite formed per mole of oxygen diffused through the layer,

$$(\Delta x)^2 = -2\bar{D}_O \frac{\Delta G^0_{Fe_2SiO_4}}{RT} t. \quad (11)$$

If, by contrast, $D_{Fe} \ll D_{Si} \ll D_O$, we could perform a similar calculation to show that

$$(\Delta x)^2 = -2\bar{D}_{Si} \frac{\Delta G^0_{Fe_2SiO_4}}{RT} t. \quad (12)$$

(c) Counterdiffusion of Iron and Silicon

If we assume that oxygen is essentially immobile within the fayalite, so that growth occurs by counterdiffusion of iron and silicon within the fayalite, the fluxes of the iron and silicon will be coupled to maintain stoichiometry:

$$j_{Fe^{2+}} = -2j_{Si^{4+}}.$$

From (3a) and (3c) we can show that

$$j_{Fe^{2+}} = -2j_{Si^{4+}} = \frac{-2}{RT} \frac{D_{Fe} C_{Fe} D_{Si} C_{Si}}{D_{Fe} C_{Fe} + 4 D_{Si} C_{Si}} \cdot \frac{(2 d\mu_{Fe^{2+}} - d\mu_{Si^{4+}})}{dx}.$$

As $2Fe^{2+} + 2SiO_2 \rightleftarrows Fe_2SiO_4 + Si^{4+}$,

$$2\mu_{Fe^{2+}} - \mu_{Si^{4+}} = \mu_{Fe_2SiO_4} - 2\mu_{SiO_2}.$$

Since $d\mu_{Fe_2SiO_4} = 0$ across the fayalite layer,

$$2 d\mu_{Fe^{2+}} - d\mu_{Si^{4+}} = -2 d\mu_{SiO_2}.$$

Thus, assuming that $D_O \ll D_{Fe} \ll D_{Si}$, and following similar arguments to those presented above, we can show that, as $2C_{Si} = C_{Fe} = 2/V_m$ and $\xi = 1$ mole of fayalite formed per mole of iron diffused through the layer ($\frac{1}{2}$ mole due to diffusion of Fe^{2+} and $\frac{1}{2}$ mole due to counterdiffusion of $\frac{1}{2}Si^{4+}$),

$$(\Delta x)^2 = -4\bar{D}_{Fe} \frac{\Delta G^0_{Fe_2SiO_4}}{RT} t. \quad (13)$$

Conversely, if $D_O \ll D_{Si} \ll D_{Fe}$, the thickness of the layer will follow

$$(\Delta x)^2 = -8\bar{D}_{Si} \frac{\Delta G^0_{Fe_2SiO_4}}{RT} t. \quad (14)$$

Therefore, depending on the relative rates of diffusion of the ionic species within the fayalite, one of six possible situations will predominate, permitting the mean effective diffusivity of the rate-limiting species to be calculated from measurements of fayalite layer thickness as a function of time and using (9) through (14). The values of the Gibbs free energy of formation for fayalite from the oxides $\Delta G^0_{Fe_2SiO_4}$ were taken from Robie et al. (1978).

Diffusion Path

Throughout these calculations, we have referred to the effective chemical diffusivities of the ionic species that constitute the fayalite with no attempt to address possible diffusion paths. The diffusivities have been treated as though the transport were occurring uniformly through the fayalite layer. Although these bulk diffusivities would represent true chemical diffusion coefficients if lattice diffusion dominated transport, this situation may not be the case in this study, where fast diffusion pathways may exist along the grain boundaries. To determine the mean grain boundary diffusivity $\bar{D}_i^{gb}$ from the mean effective diffusivity $\bar{D}_i$ for the species i that regulates the growth of the fayalite, corrections must be made for the grain size of the fayalite d, and the width of the diffusion path (the effective grain boundary width δ), through

$$\bar{D}_i^{gb} = \bar{D}_i \frac{d}{\delta}. \quad (15)$$

Although this relation is based on a parallel model of grain boundaries that does not consider the tortuosity of the diffusion path (Brady 1983), incorporation of a tortuosity term in (15) will affect the calculated grain boundary diffusivity by less than a factor of two. Thus, we can determine $\bar{D}_i^{gb}\delta$ from $\bar{D}_i$ if we can measure d, assuming that the flux of the rate-limiting species is predominantly along the grain boundaries.

Experimental Methods

Samples of natural single-crystal quartz, which were optically clear and inclusion-free, were prepared as thin slices (approximately $1 \times 3 \times 3$ mm^3) and polished with 1 μm alumina. These samples were packed in iron oxide and reacted at temperatures from 1000° to 1120° C under controlled oxygen fugacity conditions at 1 atm total pressure. The f_{O_2} was controlled using CO/CO_2 gas mixtures and monitored with a zirconia oxygen cell adjacent to the sample. Fugacities were chosen to be within either the wüstite or the magnetite stability fields with f_{O_2} from $10^{-9.9}$ to $10^{-13.0}$ atm at 1120° C. These conditions are within the fayalite stability field as defined by O'Neill (1987) (Fig. 1). Experimental durations ranged from 4 to 200 hours.

Hematite, which had been preannealed at 900° C in air and lightly ground, was generally used as the starting oxide phase around the quartz plates; sufficient powder was used that the cylinder of densified oxide around the quartz after each experiment was about 10 mm in diameter and 8 mm thick. The high initial porosity of the oxide powders permitted easy transport of oxygen out of the oxide as it equilibrated within either the magnetite or wüstite stability regions. This reduction of hematite provided fine grain size and sufficient contact to form a coherent initial interface between the quartz and the oxide, which proved to be critical in generating a uniform fayalite rim. In many of the experiments, the quartz samples were placed on top of a fully dense wüstite or magnetite wafer, and in some experiments wüstite or magnetite powders were substituted for hematite as starting materials. The results of these latter experiments agreed well with those utilizing annealed hematite powder. A moderate static load (0.7 MPa) was applied perpendicular to the large faces of the quartz, using Al_2O_3 pistons, to aid in densification of the iron oxide, and to increase the initial contact area between the oxide and the quartz.

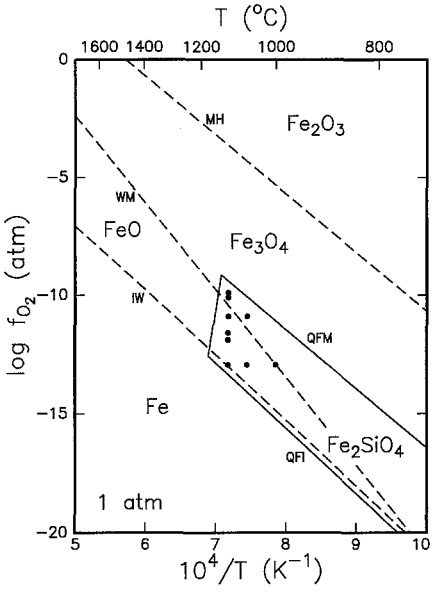

Fig. 1. Phase diagram for fayalite and the iron-oxygen system. The stability field for fayalite is indicated by the *solid lines*, where QFI is the quartz-fayalite-iron and QFM is the quartz-fayalite-magnetite phase boundary (O'Neill 1987). The stability fields for the various iron oxides and metallic iron are bounded by the *dashed lines*, where IW is the iron-wüstite, WM is the wüstite-magnetite, and MH is the magnetite-hematite phase boundary (Schwab and Küstner 1981; O'Neill 1988). The *filled circles* indicate the oxygen fugacities and temperatures for these experiments

Following the experiments, samples were cut in half with a diamond saw. One half was then mounted in epoxy, and polished with 1 μm alumina powder. In several cases, the other half was used for repeat experiments as an additional check of reproducibility. The iron oxide, quartz and fayalite were easily distinguished by their contrasting reflectivities under reflected light microscopy (Fig. 2). The thickness of the fayalite was measured at a minimum of 100 points along the rim for each sample; a mean and standard deviation were calculated from these measurements for each temperature, time, and oxygen fugacity on the assumption of a normal frequency distribution. The identity and morphology of the reaction phase was confirmed using a Cameca SX-50 electron microprobe and an International Scientific Instruments SX-40 scanning electron microscope (SEM). The grain size of the fayalite was measured from SEM images of the fayalite rims after etching in concentrated HCl.

Results

In several experiments using hematite powders that had not been preannealed in air and in a number of others using wüstite powders, a widely dispersed fayalite phase was observed throughout the iron oxide near the quartz surface (Fig. 3a). This morphology is consistent with the results reported by Schmalzried (1978) for the formation of Co_2SiO_4 from a CoO single crystal and SiO_2 powder. Schmalzried attributed this morphology to fast surface or vapor phase transport early in the experiment before the SiO_2 densified near the CoO crystal. We have solved this problem by using heat-treated hematite powders and/or fully dense wüstite wafers, and by applying a light load to the powders to improve densification. Although the reasons for the difference in morphology are not completely understood, it appears that the formation of a coherent fayalite rim early in the experiment is critical in establishing diffusion-limited kinetics. A several micron intercept at zero time for all experiments reflects the initial rapid formation of the reaction rim. All calculations of diffusivity are based on experiments in which uniform, coherent rims were formed.

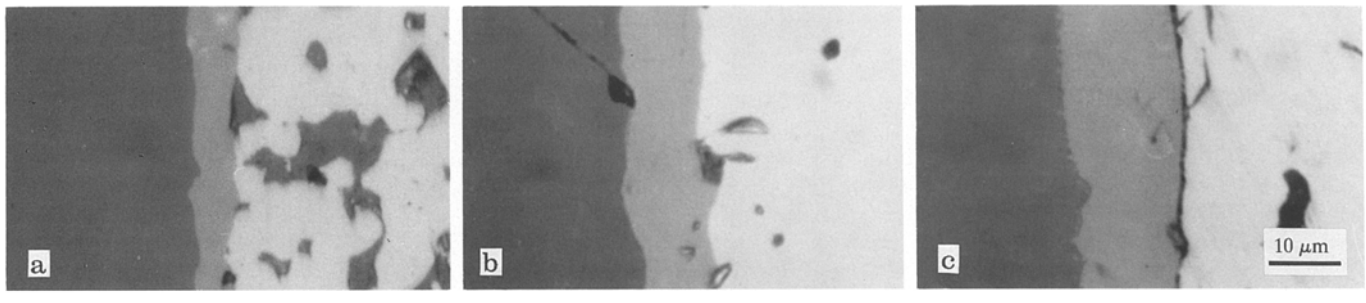

Fig. 2. Reflected light, optical micrographs of fayalite rims (medium gray phase), grown by the reaction between quartz (*left*, dark phase) and magnetite (*right*, light phase) at an f_{O_2} of $10^{-9.9}$ atm and 1120° C for **a** 20 h, **b** 100 h, and **c** 200 h. The dark gray phase between the magnetite grains in **a** is epoxy, injected after the experiments. A 10 μm scale bar for the three micrographs is shown in the *bottom right* of **c**

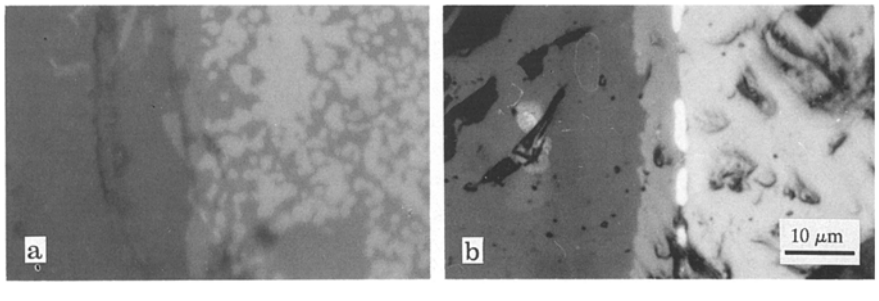

Fig. 3. Reflected light, optical micrographs of **a** a dispersed fayalite phase (medium gray) throughout the wüstite (*right*, light phase) from an experiment in which a stable rim did not form; the dark phase on the *left* is quartz; **b** a fayalite rim that was grown with an inert platinum marker, shown as the discontinuous bright spots along the wüstite-fayalite interface. A 10 μm scale bar is shown on the *bottom right* of **b**

Table 1. Experimental conditions and rate constants for fayalite growth experiments

Run No.	T(°C)	t(h)	$\log f_{O_2}$ (atm)	Δx (μm)
QFM 11	1120	10	−9.97	4.6±1.9
QFM 16	1120	20	−9.92	6.1±1.3
QFM 14	1120	40	−9.96	7.8±1.7
QFM 12	1120	100	−9.97	11.1±1.9
QFM 12a	1120	200	−9.93	14.5±2.7
			−9.95±0.02	k=0.98±0.04 μm²/h
QFM 39	1120	4	−10.10	4.9±1.7
QFM 21	1120	10	−10.12	6.6±1.9
QFM 22	1120	20	−10.15	7.1±1.7
QFM 40	1120	20	−10.08	8.7±2.8
QFM 26	1120	40	−10.13	8.8±1.9
QFM 58	1120	60	−10.13	9.1±2.0
			−10.12±0.03	k=0.94±0.31 μm²/h
QFM 15	1120	10	−10.97	5.6±1.2
QFM 42	1120	10	−11.00	5.2±2.2
QFM 41	1120	20	−10.80	8.7±2.7
QFM 57	1120	40	−10.96	7.9±1.8
QFM 46	1120	40	−10.92	7.9±2.5
QFM 47	1120	100	−10.89	13.9±3.4
			−10.92±0.07	k=1.71±0.26 μm²/h
QFM 70	1070	10	−10.90	4.6±1.9
QFM 72	1070	50	−10.91	7.0±2.6
QFM 71	1070	100	−10.90	9.2±3.6
			−10.90±0.01	k=0.71±0.05 μm²/h
QFM 23	1120	10	−11.60	6.5±1.6
QFM 24	1120	20	−11.60	11.1±3.2
QFM 25	1120	40	−11.66	10.1±2.9
QFM 75	1120	100	−11.63	16.5±2.0
			−11.63±0.3	k=2.31±0.53 μm²/h
QFM 34	1120	10	−11.80	7.7±2.6
QFM 5	1120	10	−11.80	6.8±2.7
QFM 44	1120	10	−11.95	5.9±1.9
QFM 13	1120	20	−11.80	7.0±1.3
QFM 33	1120	20	−11.80	9.2±2.1
QFM 17	1120	20	−11.80	10.0±3.3
QFM 6	1120	40	−11.85	12.8±5.4
QFM 18	1120	40	−11.82	14.7±4.6
QFM 73	1120	50	−11.95	11.2±3.4
QFM 66	1120	100	−11.95	14.7±4.6
QFM 7	1120	100	−11.80	16.1±4.3
			−11.83±0.07	k=2.09±0.37 μm²/h
QFM 52	1120	5	−12.97	5.5±1.7
QFM 54	1120	7	−12.96	6.6±1.9
QFM 48	1120	10	−12.96	9.0±2.1
QFM 49	1120	40	−12.97	13.1±3.5
QFM 53	1120	88.5	−12.98	16.8±1.8
			−12.97±0.01	k=2.91±0.29 μm²/h
QFM 51	1070	14.5	−12.98	5.7±1.8
QFM 50	1070	40	−12.96	7.9±2.5
QFM 61	1070	60	−12.97	10.0±2.6
			−12.97±0.01	k=1.46±0.18 μm²/h
QFM 43	1000	100	−12.98	4.0±1.7
QFM 74	1000	200	−12.94	5.3±0.7
			−12.96±0.03	k=0.12 μm²/h

The rims are composed of a layer of dense, fine-grained, polycrystalline fayalite, which increased in thickness with experimental duration (Fig. 2). Observations in the SEM of etch surfaces indicated a grain size in the range 0.1 to 0.5 μm for all experimental durations. Although we did not attempt a detailed statistical analysis, the average grain size of the fayalite did not increase by more than a factor of 2 with increase in experimental duration from 10 to 100 h. Thickness and morphology of the rims showed no dependence on the crystallographic orientation of the quartz, as might have been expected if the growth of the rim were interface-controlled. The quartz was cracked in most samples after the experiments, but this cracking appears to have occurred during cooling of the sample, as no fayalite was observed in the cracks. In experiments for which samples with previously formed rims were used as starting samples, the fayalite did grow into the cracks that already existed in the quartz.

Mean rim thicknesses and error bars, computed as one standard deviation from the mean, for all experiments are listed in Table 1. The most complete set of experiments was performed at a temperature of 1120° C, over ranges of oxygen fugacity and experimental duration. Figure 4a shows the square of the rim thickness versus time for three oxygen fugacities; the square of the rim thickness Δx^2 increases linearly with time for all oxygen fugacities, and the rate of rim growth increases with decreasing oxygen fugacity at constant temperature. We applied linear least squares regressions to the rim thickness data as a function of time for each set of f_{O_2} and temperature conditions. Rate constants k were determined as the slopes of the fits and are given in Table 1; the errors in k were determined as one standard deviation of the data from the fitted line. These rate constants are related to the mean effective diffusivities of the rate-limiting species by (9) through (14), depending on the relative diffusion rates of iron, oxygen and silicon. Figure 4b shows a plot of Δx^2 versus t for temperatures of 1000°, 1070°, and 1120° C at $f_{O_2}=10^{-13.0}$ atm; the rate of growth increases with increasing temperature at constant f_{O_2}. Although, within the error of the data, the same $t=0$ intercept is obtained for all oxygen fugacities at 1120° C, the initial rim thickness appears to increase with increasing temperature.

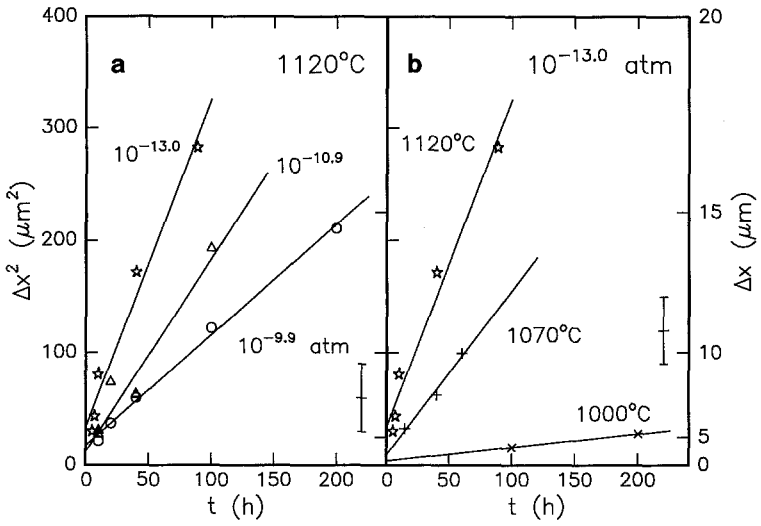

Fig. 4. Rim thickness versus the square root of time for **a** samples annealed at a range of oxygen fugacities at 1120° C, and **b** samples annealed at a range of temperatures at an f_{O_2} of $10^{-13.0}$ atm (in the wüstite stability field). For clarity, only the data for three of the six oxygen fugacities were plotted in **a**. The *solid lines* were fitted to the data using a linear least squares regression. The error bars in the *lower right* of each figure represent typical error bars for the data

In order to determine the direction of rim growth, and hence of the mobile ionic species, several experiments were performed in which a small amount of platinum paint was applied to the surface of the quartz. The effectiveness of an inert marker in locating the initial contact depends on the coherence of the marker with the surface, and requires that it not inhibit the diffusion. In general, the results show platinum lining the interface between the fayalite and the iron oxide (Fig. 3b). Although this observation is generally true, platinum was sometimes found in the interior of the fayalite.

Discussion

The experimental data on the rate of growth of fayalite by the reaction between iron oxide and quartz at various oxygen fugacities and temperatures show clear correlations of increased growth rate with increasing temperature and decreasing oxygen fugacity. The growth of the fayalite rims is consistent with a parabolic rate law, indicating diffusion-controlled growth. Using the diffusion rates calculated from the rate constants for the various relative ionic diffusivities, analyses of their dependencies on temperature and oxygen fugacity, and observations of the morphology of the fayalite rims, we can determine the defect speciation, transport path, and diffusion rate of the ionic species that regulates the growth of fayalite in these experiments.

Morphological Constraints

The platinum inert marker experiments have shown that, in general, the growth of the fayalite occurs at the quartz-fayalite interface, indicating that iron and oxygen are the more mobile species in the fayalite rim. In addition, the wavy morphology of the fayalite-quartz interface is suggestive that rim formation occurs there. It is noteworthy that, since the grain boundaries are formed *in situ* at temperature, we avoid the difficulties associated with microcracking along pre-existing grain boundaries during heating, with the resultant complication of fast transport paths for oxygen.

Thermochemical Constraints

Mean effective diffusivities may be determined as a function of f_{O_2} and T from the measured rate constants for the various relative diffusivity cases using (9) through (14). Figure 5a shows mean effective diffusivities calculated from the rate constants for three temperatures at an f_{O_2} of $10^{-13.0}$ atm, using (9) ($D_{Si} \ll D_O \ll D_{Fe}$). A linear least squares regression fit to these data (line 2) yields an activation energy for diffusion-controlled growth of 540 ± 30 kJ/mol. As this activation energy was determined from only a limited data set over a narrow range of temperatures, the quoted error bars probably overestimate the accuracy of this result. A second measure of the activation energy was made at an f_{O_2} of $10^{-10.9}$ atm, but for only two temperatures (1070° and 1120° C), yielding 462 kJ/mol.

If iron diffusion regulates the growth of fayalite, the effective diffusivity for iron would be given by lines 1 or 3 on Fig. 5a, depending on whether silicon or oxygen were essentially immobile. The measurements of the diffusivity for iron in fayalite by Hermeling and Schmalzried (1984), extrapolated to $10^{-13.0}$ atm, show good agreement with our predictions if the relative diffusivities in fayalite were given by $D_{Si} \ll D_{Fe} \ll D_O$ (line 1). However, their results indicate that the diffusivity for iron increases with increasing f_{O_2} (Fig. 5b), in contradiction with our results that show a negative dependence. Consequently, under more oxidizing conditions, their measurements yield diffusivities that are considerably faster than ours. If, at the finer grain sizes in our experiments, iron transport occurred predominantly along the grain boundaries, the bulk diffusion coefficient for iron would be even faster than that predicted from Hermeling and Schmalzried (1984). Thus, it seems likely that iron is the fastest diffusing species.

If oxygen diffusion regulates the growth of fayalite, the mean effective diffusivity for oxygen would be given by line 2 in Fig. 5a; if silicon were rate-limiting, its mean

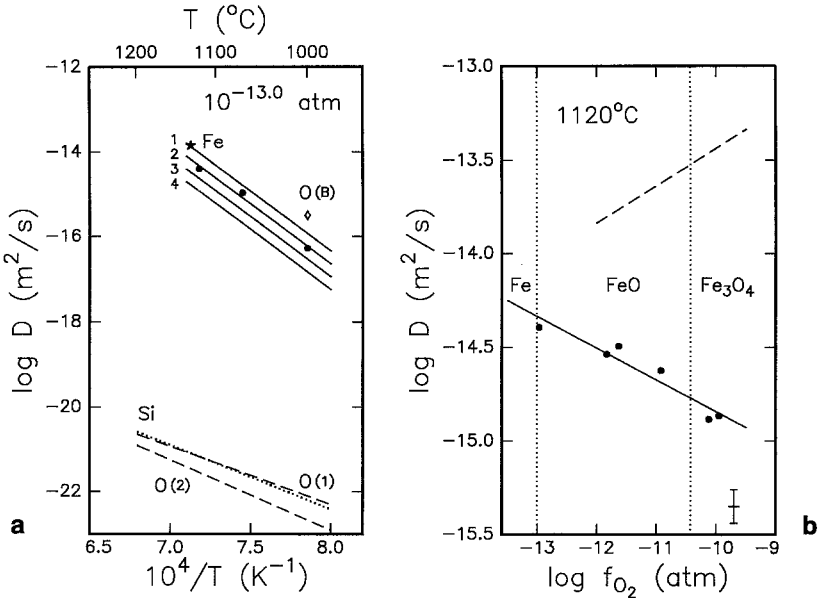

Fig. 5. a Log diffusivity versus inverse temperature for an f_{O_2} of $10^{-13.0}$ atm. The *solid lines* correspond to the following relative diffusivities of iron, oxygen and silicon, calculated from the measured rate constants: *line 1:* $D_{Si} \ll D_{Fe} \ll D_O$; *line 2* and the data points: $D_{Si} \ll D_O \ll F_{Fe}$ or $D_{Fe} \ll D_O \ll D_{Si}$ or $D_{Fe} \ll D_{Si} \ll D_O$; *line 3:* $D_O \ll D_{Fe} \ll D_{Si}$; and *line 4:* $D_O \ll D_{Si} \ll D_{Fe}$, where the intermediate diffusing species regulates growth. The diffusivity calculated assuming $D_{Si} \ll D_O \ll D_{Fe}$ from the measurements of fayalite growth by Becker et al. (1992) at $f_{O_2} = 10^{-13.3}$ atm is shown as O(*B*). Also shown is the diffusivity for iron in polycrystalline fayalite (Fe) predicted from the measurements of Hermeling and Schmalzried (1984); O(1) and O(2) indicate lattice diffusivities for oxygen in Fo_{90} olivine extrapolated from the measurements of Ryerson et al. (1989) and Gerard and Jaoul (1989); and Si indicates lattice diffusivities for silicon in Fo_{90} extrapolated from the results of Houlier et al. (1990). **b** Log diffusivity versus log f_{O_2} showing diffusivities calculated from the rate constants at 1120° C, assuming that oxygen is the rate-limiting species for fayalite growth. The *solid line* indicates the linear least squares fit to the data. The *dashed line* shows the extrapolation to pure fayalite of the 1130° C data of Hermeling and Schmalzried (1984) for iron in $Fo_{10} - Fo_{80}$ olivine. The *vertical dotted lines* indicate the boundaries between the iron, wüstite and magnetite fields

effective diffusivity would be given by lines 2 or 4, depending on whether iron or oxygen were essentially immobile. A comparison of these diffusion rates with previous measurements of lattice diffusivities in Fo_{90} olivine (Fig. 5a) indicates that lattice diffusion rates are orders of magnitude slower than our results. This disparity is unlikely to result from the difference in iron content between fayalite and Fo_{90} olivine. Thus, from morphological and thermochemical observations, it seems likely that the growth of the fayalite layer occurs by the motion of iron and oxygen, and is rate-limited by the diffusion of oxygen ions along the grain boundaries.

The activation energy for fayalite growth (540 kJ/mol) is somewhat larger than those measured for iron/magnesium diffusion in fayalite (210–255 kJ/mol) (Misener 1974; Buening and Buseck 1973), oxygen (266–318 kJ/mol) and silicon (291 kJ/mol) lattice diffusion in olivine (Gerard and Jaoul 1989; Ryerson et al. 1989; Houlier et al. 1990), and oxygen grain boundary diffusion in dunite (356 kJ/mol) (Watson 1986). Although, qualitatively, our activation energy is closest to that measured for oxygen grain boundary diffusion in olivine, we do not feel that our result is sufficiently well-constrained to use as a criterion for discriminating between the possible rate-limiting species in the growth of fayalite.

The dependence of growth rate on oxygen fugacity provides additional constraints on both the rate-limiting species and on the structural defect that controls the diffusion process. Figure 5b shows the mean effective diffusivity of oxygen as a function of oxygen fugacity, assuming $D_{Si} \ll D_O \ll D_{Fe}$; a linear least squares fit to the data yields an f_{O_2} exponent of $m = -0.17 \pm 0.02$ ($\sim 1/6$). Although the absolute diffusivity might be different if another species were rate-limiting, the f_{O_2} exponent would not be affected.

The diffusivity of an ionic species in a crystal lattice is given by the diffusivity of the associated defect multiplied by the concentration of that defect. Since, by the dilute solution approximation, the diffusivity of a defect species at low concentrations is independent of the chemical environment, the effects of chemical environment on diffusion of an ionic species result predominantly from its influence on defect concentrations. The dependence of defect concentrations in fayalite on the chemical environment has been derived by Sockel (1974) from knowledge of the crystal and defect structure of the transition metal oxides, combined with electrical conductivity and gravimetric measurements. The most likely defects in fayalite, using the notation of Kroger and Vink (1956), are normally charged vacancies (V''_{Fe}, V''''_{Si}, $V^{\bullet\bullet}_O$) and interstitials ($Fe^{\bullet\bullet}_i$, $Si^{\bullet\bullet\bullet\bullet}_i$, O'_i), and ferric iron (Fe^{3+}) substitution on octahedral cation sites ($Fe^{\bullet}_{Fe}$). According to electrical conductivity and gravimetric experiments reported by Sockel (1974), the majority defects in fayalite throughout its stability field at 1120° C are V''_{Fe} and $Fe^{\bullet}_{Fe}$, so that charge neutrality is established by

$$2[V''_{Fe}] = [Fe^{\bullet}_{Fe}],$$

where the brackets indicate concentration of the defect species. Using this information, the dependencies of all defect concentrations can be derived in terms of the thermodynamic parameters. As only the concentrations of positively charged defects decrease with increasing f_{O_2} ($[Fe_i^{\bullet\bullet\bullet}] \propto f_{O_2}^{-1/6} a_{FeO}^{1/3}$, $[V_O^{\bullet\bullet}] \propto f_{O_2}^{-1/6} a_{FeO}^{-2/3}$, $Si_i^{\bullet\bullet\bullet\bullet} \propto f_{O_2}^{-1/3} a_{FeO}^{-10/3}$), these are the most likely candidates for the species that regulates fayalite growth in these experiments. Since our experiments were performed in a gradient in oxide activity, we could not measure the dependence of diffusion on a_{FeO}.

Given that the growth of fayalite is regulated by the grain boundary diffusion of oxygen, the sign and magnitude of the f_{O_2} dependence is consistent with transport by a vacancy mechanism. Although the lattice diffusion of oxygen in Fo_{90} olivine shows a positive dependence on f_{O_2}, indicating an interstitial diffusion mechanism (Gerard and Jaoul 1989; Ryerson et al. 1989), the transport process may be different in fayalite. In addition, the difference in the energetics between lattice and grain boundary defects may result in a change from interstitial diffusion in the lattice to vacancy diffusion along the grain boundaries for the same species. Even though defects other than the normally charged vacancies and interstitials may exist in fayalite, they are unlikely to occur in sufficient concentrations to contribute to ionic diffusion. We also note that the theoretical relationship between defect concentrations and the thermodynamic parameters were calculated for lattice defects and they may only be applied to grain-boundary regions of single-phase aggregates with caution.

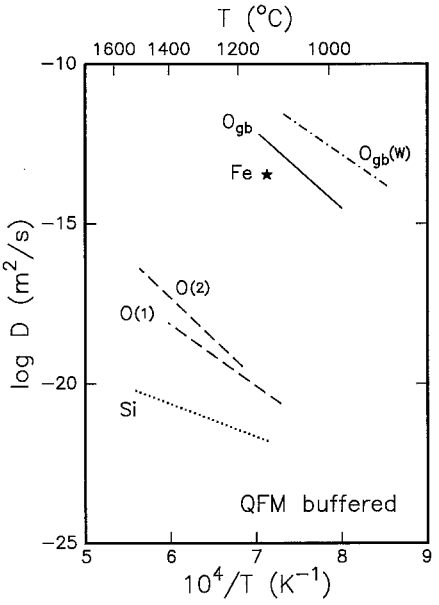

Fig. 6. Log diffusivity versus inverse temperature for a number of ionic species in fayalite and Fo_{90} olivine. Our results for the mean grain boundary diffusivity of oxygen in fayalite are labelled O_{gb}; $O_{gb}(W)$ indicates the grain boundary diffusivity for oxygen in olivine polycrystals as determined by Watson (1986); Fe indicates the diffusivity for iron in polycrystalline fayalite by Hermeling and Schmalzried (1984); and O(1), O(2), and Si indicate the lattice diffusivities for oxygen (Ryerson et al. 1989; Gerard and Jaoul 1989) and silicon (Houlier et al. 1990) in olivine. All data are plotted for oxygen fugacities buffered at quartz-fayalite-magnetite (QFM), except for the Watson (1986) data, which where measured in an oxygen potential gradient

Transport Mechanism

The bulk of the evidence, including the magnitude of the diffusivity, the dependence on oxygen fugacity, the position of platinum markers, and the general morphology of the fayalite strongly favor one model for fayalite formation: the fayalite grows by the transport of iron and oxygen from the iron oxide phase through the fayalite to react at the quartz-fayalite interface. The rate of fayalite growth is controlled by the grain boundary diffusion of oxygen, probably by a vacancy mechanism. Using a novel Mössbauer technique, Becker et al. (1992) also measured the rate of growth of fayalite from the reaction between FeO and SiO_2 (in their case, quartz glass). From their measurements, they determined a parabolic rate constant of $k_p = 10^{-16}\ m^2\ s^{-1}$ at 1000° C and an f_{O_2} of $10^{-13.3}$ atm. Assuming that the same growth mechanism occurred in their samples, this result indicates a mean effective diffusivity for oxygen that is similar to our result at approximately the same conditions (Fig. 5a).

Using our rate constants, and (9) and (15) we can determine mean grain-boundary diffusivities for oxygen in fayalite. In this context, "mean" refers to the fact that the diffusivity is measured in a gradient of a_{FeO}. If we use the measured grain size of $d = 0.25\ \mu m$, the mean grain boundary diffusion rate for oxygen in fayalite $\bar{D}_O^{gb}$ (in $m^2\ s^{-1}$) is given by

$$\bar{D}_O^{gb}\delta = (1.28 \pm 0.11) \times 10^{-3} f_{O_2}^{-0.17 \pm 0.02} e^{-540 \pm 30/RT},$$

where the activation energy is expressed in kJ/mol. Using this relationship and assuming a grain boundary width of $\delta = 1$ nm (Ricoult and Kohlstedt 1983), we have plotted the mean oxygen grain boundary diffusivity in fayalite in Fig. 6. This relationship yields diffusivities that are a factor of about 30 × slower than the mean grain boundary diffusivities for oxygen in Fo_{90} olivine polycrystals, determined by Watson (1986) at a pressure of 1 GPa using an oxygen potential gradient as the driving force for diffusion ($O_{gb}(W)$ in Fig. 6). This disparity is larger than can be accounted for by the differences in mean f_{O_2} and a_{FeO} in the two experimental systems, but may reflect a contribution due to short-circuit diffusion by vapor transport in open grain boundaries in his samples, or fundamental differences in grain boundary structure between the two minerals.

Acknowledgements. Support of the National Science Foundation through grant EAR-9018044, and of the Pennsylvania State University Faculty Research Fund, is gratefully acknowledged. We wish to thank David Kohlstedt for his assistance in deriving the thermodynamic rate laws, and for many fruitful discussions. Mark Angelone assisted with the microprobe analyses. Critical reviews by Rudiger Dieckmann, Bruce Watson, and Bill Durham greatly improved the manuscript. This research also benefitted from numerous discussions with Jeff Lawlis.

References

Atkinson A (1987) Grain boundary diffusion in oxides and its contribution to oxidation processes. In: Oxidation of metals and associated mass transport, Dayananda MA, Rothman SJ, King WE (eds). The Metallurgical Society, Inc., pp 29–47

Atkinson A, Taylor RI (1979) The diffusion of nickel in the bulk and along dislocations in NiO single crystals. Philos Mag 39:581–595

Atkinson A, Taylor RI (1981) The diffusion of ^{63}Ni along grain boundaries in nickel oxide. Philos Mag 43:979–998

Atkinson A, Taylor RI (1982) The diffusion of ^{57}Co along grain boundaries in nickel oxide. Philos Mag 45:583–592

Atkinson A, Taylor RI (1985) Diffusion of ^{55}Fe in Fe_2O_3 single crystals. J Phys Chem Solids 46:469–475

Becker KD, Dreher S, Wißmann (1992) A high-temperature Mössbauer study of fayalite, Fe_2SiO_4: Cation diffusion and reactivity. Ber Bunsenges Phys Chem 96:1778–1783

Borchardt G, Jaoul O, Scherrer S (1979) Formazione di silicati mediante reazioni allo stato solido ad alta temperatura. La Ceram Nov–Dec:7–22

Brady JB (1983) Intergranular diffusion in metamorphic rocks. Am J Sci 283A:181–200

Buening DK, Buseck PR (1973) Fe–Mg lattice diffusion in olivine. J Geophys Res 78:6852–6862

Farver JR, Yund RA (1991) Measurement of oxygen grain boundary diffusion in natural, fine-grained, quartz aggregates. Geochim Cosmochim Acta 55:1597–1607

Gerard O, Jaoul O (1989) Oxygen diffusion in San Carlos olivine. J Geophys Res 94:4119–4128

Hermeling J, Schmalzried H (1984) Tracerdiffusion of the Fe-cations in olivine $(Fe_xMg_{1-x})_2SiO_4$(III). Phys Chem Minerals 11:161–166

Houlier B, Jaoul O, Abel F, Liebermann RC (1988) Oxygen and silicon self-diffusion in natural olivine at 1300° C. Phys Earth Planet Ints 50:240–250

Houlier B, Cheraghmakani M, Jaoul O (1990) Silicon diffusion in San Carlos olivine. Phys Earth Planet Ints 62:329–340

Jaoul O, Froidevaux C, Durham WB, Michaut M (1980) Oxygen self-diffusion in forsterite: Implications for the high-temperature creep mechanism. Earth Planet Sci Lett 47:391–397

Jaoul O, Houlier B (1983) Study of ^{18}O diffusion in magnesium orthosilicate by nuclear microanalysis. J Geophys Res 88:631–624

Jaoul O, Poumellec M, Froidevaux C, Havette A (1981) Silicon diffusion in forsterite: A new constraint for understanding mantle deformation. In: Anelasticity in the earth; geodynamic series; volume 4, Stacey FD, Paterson MS, Nicholas A (eds). Am Geophys Union, Washington DC, pp 95–100

Jurewicz AJG, Watson EB (1988) Cations in olivine, Part 2: Diffusion in olivine xenocrysts, with applications to petrology and mineral physics. Contrib Mineral Petrol 99: 186–201

Kroger FA, Vink HJ (1956) Relations between the concentrations of imperfections in crystalline solids. In: Solid State Physics, Vol 3, Seitz F, Turnball D (eds). Acad Press, New York, pp 307–435

Misener DJ (1972) Interdiffusion studies in the system Fe_2SiO_4 $-Mg_2SiO_4$. Ann Rep Geophys Lab Yearb 71:54–56

Misener DJ (1974) Cationic diffusion in olivine to 1400° C and 35 kbar. In Geochemical Transport and Kinetics. eds Hofmann AW, Giletti BJ, Yoder HS, Yund RA, pp 117–129. Carnegie Inst Wash 634

Nakamura A, Schmalzried H (1984) On the Fe^{2+} $-Mg^{2+}$-interdiffusion in olivine (II). Ber Bunsenges Phys Chem 88:140–145

O'Neill HStC (1987) Quartz-fayalite-iron and quartz-fayalite-magnetite equilibria and the free energy of formation of fayalite (Fe_2SiO_4) and magnetite (Fe_3O_4). Am Mineral 72:67–75

O'Neill HStC (1988) Systems Fe–O and Cu–O: Thermodynamic data for the equilibria Fe–"FeO", Fe–Fe_3O_4, "FeO" $-Fe_3O_4$, Cu–Cu_2O, and Cu_2O–CuO from emf measurements. Am Mineral 73:470–486

Reddy KPR, Oh SM, Major Jr LD, Cooper AR (1980) Oxygen diffusion in forsterite. J Geophys Res 85:322–26

Ricoult DL, Kohlstedt DL (1983) Structural width of low-angle grain boundaries in olivine. Phys Chem Minerals 9:133–138

Robie RA, Hemingway BS, Fisher JR (1978) Thermodynamic properties of minerals and related substances at 298.15 K and 1 bar (10^5 Pascals) pressure and at higher temperatures. United States Printing Office, Geological Survey Bulletin 1452, Washington

Ryerson FJ, Durham WB, Cherniak DJ, Lanford WA (1989) Oxygen diffusion in olivine: Effect of oxygen fugacity and implications for creep. J Geophys Res 94:4105–4118

Schmalzried H (1978) Reactivity and point defects of double oxides with emphasis on simple silicates. Phys Chem Minerals 2:279–294

Schwab RG, Küstner D (1981) Die Gleichgewichtsfugazitäten technologisch and petrologisch wichtiger Sauerstoffpuffer. Neues Jahrb Mineral Abh 140:111–142

Sockel HG (1974) Defect structure and electrical conductivity of crystalline ferrous silicate. In: Defects and Transport in Oxides, Smeltzer MS, Jaffee RJ (eds). Plenum Press, New York, pp 341–354

Watson EB (1986) An experimental study of oxygen transport in dry rocks and related kinetic phenomena. J Geophys Res 91:14>117–14>131

Watson EB (1991) Diffusion in fluid-bearing and slightly-melted rocks: Experimental and numerical approaches illustrated by iron transport in dunite. Contrib Mineral Petrol 107:417–434